Aalborg Universitet

Integrated inductor for interleaved operation of two parallel three-phase voltage source converters

Gohil, Ghanshyamsinh; Bede, Lorand; Teodorescu, Remus; Kerekes, Tamas; Blaabjerg, Frede

Integrated Inductor for Interleaved Operation of Two Parallel Three-phase Voltage Source Converters

Ghanshyamsinh Gohil, Lorand Bede, Remus Teodorescu, Tamas Kerekes, Frede Blaabjerg
Department of Energy Technology, Aalborg University
Aalborg, Denmark
gvg@et.aau.dk
URL: http://www.et.aau.dk

Acknowledgments

Keywords

<<Voltage source converters>>, <<Magnetic integration>>, <<Parallel converters>>, <<Carrier interleaving>>, <<Integrated inductor>>, <<Interleaved inverters>>

Abstract

This paper presents an integrated inductor for two parallel interleaved Voltage Source Converters (VSCs). Interleaving of the carrier signals leads to improvement in the harmonic quality of the resultant output voltage and the line current filtering requirements can then be reduced. However, the instantaneous potential difference, caused by the interleaved carriers, may drive large circulating current between the parallel VSCs and an additional inductor is often placed in the circulating current path to suppress the current to an acceptable limit. Integration of both line filter inductor and circulating current filter inductor is proposed. The flux in the magnetic structure is analyzed and the values of the line filter inductance and circulating current filter inductance are derived. Steady-state and the transient performance of the system has been verified by means of simulation and experimental results.

Introduction

Three-phase two-level pulsewidth modulated Voltage Source Converter (VSC) is widely used in many industrial and renewable energy applications. This converter is often realized using a Si Insulated Gate Bipolar Transistor (IGBT). The VSC, with an IGBT as a switching device, suffers from excessive losses if the switching frequency is increased beyond few kHz. Due to the limited switching frequency, large line filter components are generally employed to comply with the power quality requirements. In many high power applications, several VSCs are connected in parallel to achieve the desired power/current level [1]. These parallel connected VSCs can be operated with interleaved carrier signals and multi-level voltage waveforms can be achieved.

As a result of the interleaved carriers, the switched output voltages (referred as a pole voltage hereafter) of the parallel VSC legs are phase shifted. As a result, some of the harmonic frequency components that are present in the individual pole voltages of the parallel VSC legs are also phase shifted and their contribution in the resultant output voltage is fully/partly canceled [2–5]. The improvement in the harmonic quality of the resultant output voltage leads to reduction in the line current filtering requirements. However, the difference of the phase shifted harmonic components of the pole voltages appears across the closed path and drives the circulating current between the parallel VSCs.

The flow of the circulating current between parallel VSCs increases the losses and leads to unnecessary over-sizing of the components present in the circulating current path. Therefore, it should be suppressed to an acceptable limits. An inductive component is often used, which offers high impedance to the phase shifted harmonic component of the pole voltages and thereby suppressing the circulating current. One of the ways to achieve this is to provide a strong magnetic coupling between the parallel VSC legs [3,6–9], as shown in Fig. 1. The system with parallel interleaved VSCs uses two distinct inductive components:

1. Line filter inductor (L_f) for improving the injected line current quality.
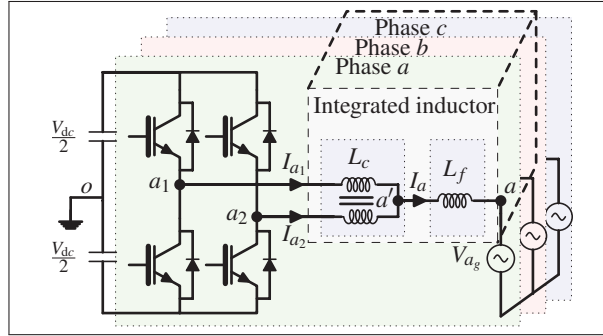2. An inductor (L_c) for suppressing the circulating current.

Figure 1: Two parallel interleaved voltage source converters with a common dc-link. Circulating current is suppressed by inductor L_c and the line filter inductor L_f provides desired inductance for line current filtering. Proposed integrated inductor combines the functionalities of both the L_c and L_f of all three phases.

The advantage offered in terms of the size reduction of the line filter component is somewhat offset by the introduction of the additional circulating current inductor. The volume of these inductive components can be reduced by integrating the functionalities of both the line filter inductor and the circulating current inductor. Moreover, the size of the magnetic component can be further reduced by integrating the inductors of all three phases in a single magnetic structure.This paper proposes such integrated inductor for two parallel connected VSCs.

Parallel Interleaved Voltage Source Converters

Two parallel VSCs with the common dc-link is shown in Fig. 1. The carrier signals of these parallel VSCs are interleaved by an interleaving angle of 180°. The harmonic performance of the switched output voltage and the behavior of the circulating current is significantly influenced by the Pulse Width Modulation (PWM) scheme used [10, 11]. Therefore, the PWM scheme is briefly discussed hereafter.

A 60° discontinuous modulation (commonly referred to as a DPWM1) is used to modulate the parallel VSCs. Each VSC leg remains clamped to the dc bus for one third period (120°) of the fundamental cycle. This clamping interval is divided into two sub-intervals of 60° each and the voltage vectors are selected to arrange these sub-intervals around the positive and the negative peak of the reference voltage waveform, as shown in Fig. 2a. For the unity power factor applications, the switching of the semiconductor device is avoided when the current through that device is near its peak value. In this manner, the switching losses can be reduced up to 50% compared to that of the continuous space vector modulation scheme. In addition, for the symmetrical interleaving, the use of the DPWM1 results in a better harmonic performance compared to the continuous space vector modulation scheme [5, 10].

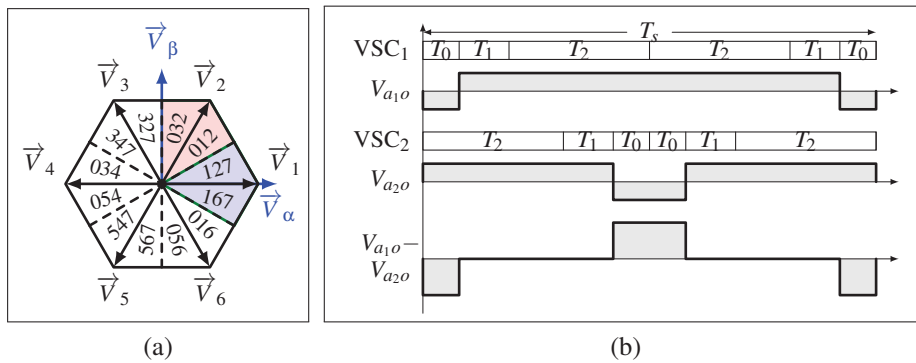| (a) | (b) |

Figure 2: Pulse width modulation scheme and the pole voltages of the parallel voltage source converters. (a) Switching sequences used in the DPWM1. The numbers represent the corresponding voltage vectors, (b) Pole voltages of phase a of both the parallel voltage source converters for the modulation index $M = 1$ and voltage space vector angle $\psi = 45°$. The interleaving angle is 180°.

The pole voltages of both the VSCs are shown in Fig. 2b. These pole voltages have the same average value. However, due to the interleaved carriers, these pole voltages are phase shifted. Therefore, there exist an instantaneous potential difference, which appears across the closed path formed due to the interleaved carriers and the parallel connection. The potential difference of the pole voltages for a particular switching interval is also shown in Fig. 2b. This potential difference drives a circulating current and the integrated inductor is used to suppress this current.

Integrated Inductor

A magnetic structure and the analysis of the integrated inductor is presented in this section.

Magnetic Structure

An integrated three-phase inductor, which combines the functionalities of the circulating current filter inductor and the three-phase line filter inductor, is proposed. The magnetic structure of the proposed inductor is shown in Fig. 3a. The flux components corresponding to each of the phases can be made
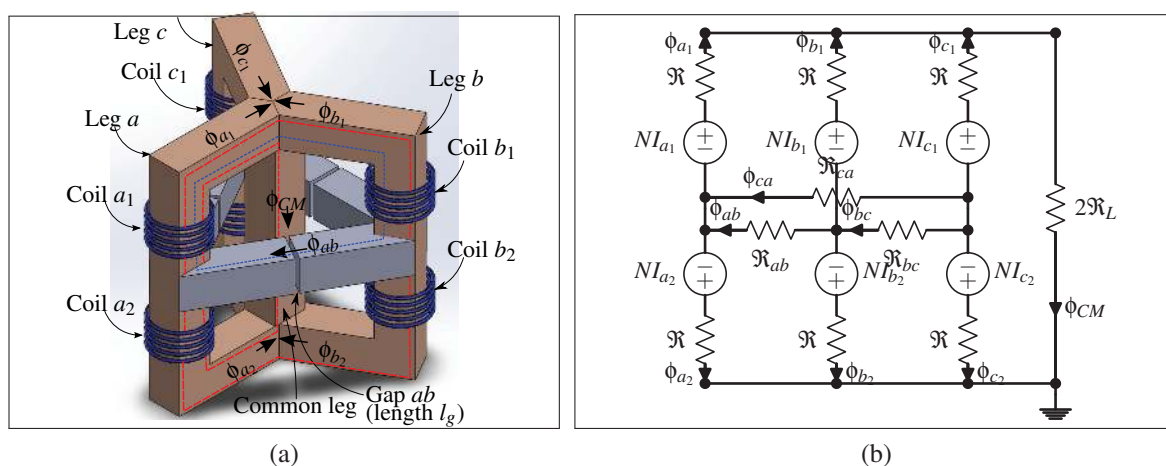

Figure 3: Three phase integrated inductor. (a) Magnetic structure, (b) Simplified reluctance model.

balance by using the symmetrical magnetic structure. The magnetic core is composed of three outer legs (referred to as a phase leg), a common leg and three bridge legs between the phases (referred to as a bridge leg). The phase leg receives both the coils of that phase. The number of turns are the same in all the coils. However, the coils corresponding to VSC_2 are wound in opposite direction than the coils of the VSC_1. The starting terminals of both the coils of a particular phase are connected to the respective output terminals of the corresponding parallel VSC legs (starting terminals of the coils of phase a are connected to the a_1 and a_2), whereas ending terminals of both the coils are connected to the common connection point (a). A high permeability material is used for the phase legs and the common leg, whereas the bridge legs are realized using the laminated iron core and the necessary air gap has been inserted in each of the bridge legs.

Simplified Reluctance Model

A simplified reluctance model of the integrated inductor is shown in Fig. 3b. The permeability of the magnetic material is assumed to be constant and the flux is assumed to be confined to the magnetic core (flux leakage is neglected). Each of the coils is represented by an equivalent magneto-motive force, which is equal to the product of the number of turns N and the current flowing through that coil. Each phase leg comprises a limb and two yokes. The reluctance of half of the limb is taken as $\Re_L$. The reluctance of each yoke is termed as $\Re_Y$. The series connection of the reluctance of the half of the limb ($\Re_L$) and the reluctance of the yoke ($\Re_Y$) is represented by the equivalent reluctance $\Re$ ($\Re = \Re_L + \Re_Y$). The equivalent reluctance of each of the bridge leg is the sum of the reluctance of the magnetic material of that bridge leg and the effective reluctance of an air gap ($\Re_{ab} = \Re_{ab_s} + \Re_{g'}$). The reluctance of the laminated steel core is very small compared to the reluctance of the air gap $\Re_{g'}$. Therefore, the reluctance of each bridge leg is approximated as $\Re_{g'}$.

By solving the reluctance network, the flux linking with the respective coils of the phase x is given as

$$\phi_{x_1} = \frac{3}{2(3\Re + 2\Re_{g'})}N(I_{x_1} + I_{x_2}) + \frac{1}{2\Re}N(I_{x_1} - I_{x_2}) - \frac{3}{8\Re}N(I_{CM,1} - I_{CM,2})$$

$$\phi_{x_2} = \frac{3}{2(3\Re + 2\Re_{g'})}N(I_{x_1} + I_{x_2}) - \frac{1}{2\Re}N(I_{x_1} - I_{x_2}) + \frac{3}{8\Re}N(I_{CM,1} - I_{CM,2})$$

(1)

where x is a subscript, which represents phases a, b, and c and $I_{CM,n}$ is the the Common Mode (CM) current of the nth VSC and it is defined as

$$I_{CM,n} = \frac{I_{a_n} + I_{b_n} + I_{c_n}}{3}$$

(2)

The flux in the common leg and the bridge leg between the phase leg a and the phase b are given as

$$\phi_{CM} = \frac{3}{8\Re_L}N(I_{CM,1} - I_{CM,2}) \text{ and } \phi_{ab} = \frac{1}{3\Re + 2\Re_{g'}}N(I_a - I_b)$$

(3)

For the parallel interleaved VSCs, the leg current can be decomposed into two distinct components

1. Resultant line current component .
2. Circulating current component.

Assuming equal current sharing between the VSCs, the leg current can be given as

$$I_{x_1} = \frac{I_x}{2} + I_{x,c} \text{ and } I_{x_2} = \frac{I_x}{2} - I_{x,c}$$

(4)

where, I_x is the resultant line current and $I_{x,c}$ is the circulating current component. Using (4), the circulating current can be obtained as

$$I_{x,c} = \frac{I_{x_1} - I_{x_2}}{2}$$

(5)

Using (2) and (5), the difference of the CM currents of the VSCs can be obtained. Since, $I_a + I_b + I_c = 0$, the CM circulating current is given as

$$I_{CM,c} = \frac{I_{CM,1} - I_{CM,2}}{2} = \frac{I_{a,c} + I_{b,c} + I_{c,c}}{3} \text{ where } n = 1,2$$

(6)

Using (1), (5), and (6) the voltage across the coils are given as

$$V_{a_1a} = V_{a_1o} - V_{ao} = -N\frac{d\phi_{x_1}}{dt} = -\frac{3N^2}{2(3\Re + 2\Re_{g'})}\frac{dI_x}{dt} - \frac{N^2}{\Re}\frac{dI_{x,c}}{dt} + \frac{3N^2}{4\Re}\frac{dI_{CM,c}}{dt}$$

(7)

$$V_{a_2a} = V_{a_2o} - V_{ao} = -N\frac{d\phi_{x_2}}{dt} = -\frac{3N^2}{2(3\Re + 2\Re_{g'})}\frac{dI_x}{dt} + \frac{N^2}{\Re}\frac{dI_{x,c}}{dt} - \frac{3N^2}{4\Re}\frac{dI_{CM,c}}{dt}$$

(8)

Line Filter Inductor L_f

Averaging of the (7) and (8) yields

$$V_{a'o} - V_{ao} = -\frac{3N^2}{2(3\Re + 2\Re_{g'})}\frac{dI_x}{dt}, \text{ where } V_{a'o} = \frac{V_{a_1o} + V_{a_2o}}{2}$$

(9)

As shown in Fig. 1, voltage $V_{a'o} - V_{ao}$ appears across the line filter inductor L_f. Therefore, from (9) the value of the line filter inductor is obtained as

$$L_f = \frac{3N^2}{4\Re_{g'} + 6\Re} \approx \frac{3N^2}{4\Re_{g'}}$$

(10)

Let the length of the air gap be l_g and the effective cross-sectional area of the air gap after considering the effects of the fringing flux be $A_{g'}$. The effective cross-sectional area of the air gap $A_{g'}$ is obtained by evaluating the cross-section area of the air gap after adding l_g to each dimension in the cross-section. Then (10) can be rewritten as

$$L_f \approx \frac{3\mu_0 N^2 A_{g'}}{4l_g}$$

(11)

Circulating Current Inductor L_c

The difference in the pole voltages of the corresponding phase drives the circulating current between the parallel VSC legs (VSC$_1$ and VSC$_2$) of that phase. This current is suppressed by inserting the inductance L_c in the circulating current path. For the proposed integrated inductor, the circulating current is described as

$$\begin{bmatrix} \Delta V_a \\ \Delta V_b \\ \Delta V_c \end{bmatrix} = \frac{N^2}{2\Re} \begin{bmatrix} 3 & -1 & -1 \\ -1 & 3 & -1 \\ -1 & -1 & 3 \end{bmatrix} \times \frac{d}{dt} \begin{bmatrix} I_{a,c} \\ I_{b,c} \\ I_{c,c} \end{bmatrix} \tag{12}$$

where $\Delta V_x = V_{x_1o} - V_{x_2o}$. As given in (12), the value of the L_c is independent of the air gap geometry and only depends on the value of the reluctance of the half of the limb ($\Re_L$) and the reluctance of the yoke ($\Re_Y$). The inductance offered to the circulating current can be increased by reducing the value of the $\Re$, which can be realized using a high permeability material for the phase legs and the common leg.

Design and Performance Comparison

The design equation for the integrated inductor is derived in this section.

Maximum Flux Density

The maximum value of the flux density in various parts of the integrated inductor is derived in this sub section.

Maximum Flux Density in Bridge Legs

Using (3) and (10), the flux in the bridge leg is given as

$$\phi_{ab} = \frac{2L_f}{3N}(I_a - I_b) \tag{13}$$

Normally the value of the L_f is chosen to limit the switch current ripple to the desired value. Let β be the ratio of the maximum switch current ripple to the rms value of the line current ($\beta = \Delta I_{x,max}/I_{x,rms}$). For the parallel interleaved VSCs with the interleaving angle of 180° and modulated using the DPWM1, the switch current ripple is maximum for $M = 1$ and for voltage space vector angle of $\psi = 0°$ [2]. The maximum switch current ripple is given as

$$\Delta I_{x,max} = \beta I_{x,rms} = \frac{V_{dc}}{24 f_c L_f} \tag{14}$$

Substituting the value of L_f and $I_a - I_b$ in (13) yields

$$\phi_{ab} = \frac{\sqrt{6}V_{dc}}{36Nf_c\beta}\cos(\psi + \theta + 30°) \tag{15}$$

where θ is the displacement power factor angle. Let, $A_{c,bl}$ be the cross section area of the bridge leg, the maximum value of the flux density in the bridge leg is given as

$$B_{bl,max} = \frac{V_{dc}}{6\sqrt{6}Nf_c\beta A_{c,bl}} \tag{16}$$

Maximum Flux Density in Common Leg

Obtaining the circulating current values from (12) and substituting in (3) yields

$$\phi_{CM} = \frac{3\Re}{2\Re_l N}\int (V_{CM,1} - V_{CM,2})dt \tag{17}$$

The flux in the common leg is proportional to the time integral of the CM voltage difference. The peak value of the $\int (V_{CM,1} - V_{CM,2})dt$ is different in every switching intervals. The maximum value out of these peak values for a given modulation index is given as

$$\int (V_{CM,1} - V_{CM,2})dt = \begin{cases} \frac{MV_{dc}}{4f_c}, & 0 \leqslant M < \frac{2}{3} \\ \frac{V_{dc}}{f_c}\left[\frac{1}{3} - \frac{M}{4}\cos\left(60° - \arcsin(\frac{1}{\sqrt{3}M})\right)\right], & \frac{2}{3} \leqslant M < \frac{2}{\sqrt{3}} \end{cases} \tag{18}$$

Over the entire modulation range, $\int (V_{CM,1} - V_{CM,2})dt$ achieves maximum value at $M = 2/3$ and the maximum value of the flux density in the common leg is given as

$$B_{CM,max} = (1 + \frac{L_y}{L_l})\frac{V_{dc}}{4Nf_cA_{c,cl}} \tag{19}$$

where $A_{c,cl}$ is the cross section area of the common leg. L_y and L_l are the mean magnetic length of the yoke and the half of the limb, respectively. It should be noted that the flux density in the common leg is maximum for $M = 2/3$. However, in many grid connected applications, the grid voltage could vary over a range of 1 ± 0.1 pu. This results in modulation index range as $0.9 \leq M \leq 1.1$. For such systems, the flux density in the common leg is maximum for $M = 0.9$ and it is given as

$$B_{CM,max}\,|_{M=0.9} = (1 + \frac{L_y}{L_l})\frac{V_{dc}}{5.466Nf_cA_{c,cl}} \tag{20}$$

Maximum Flux Density in Phase Leg

Obtaining the circulating current values from (12) and substituting it in (1) yields

$$\phi_{a_1}(t) = \frac{3N}{6\Re + 4\Re_{g'}}I_a(t) + \frac{1}{2N}\int \Delta V_a dt \tag{21}$$

Substituting the values of the $\Re_{g'}$ and I_a into (17)

$$\phi_{a_1}(t) = \frac{(\sqrt{2} + \frac{\beta}{2})V_{dc}}{24Nf_c\beta}\cos(\psi + \theta) + \frac{1}{2N}\int \Delta V_a dt \tag{22}$$

As it is evident from (22), the flux in the phase leg has two distinct components:

1. Resultant flux component $\phi_{x,r}$.
2. Circulating flux component $\phi_{x,c}$.

The displacement power factor angle is zero ($\theta = 0$) for the unity power factor applications. In this case, the resultant flux component $\phi_{x,r}$ attains its maximum value at $\psi = 0°$ and it is given as

$$\phi_{a,r_{max}} = \phi_{a,r}(t)\,|_{\psi=0°} = \frac{(\sqrt{2} + \frac{\beta}{2})V_{dc}}{24Nf_c\beta} \tag{23}$$

The circulating flux component $\phi_{x,c}$ is proportional to the $\int \Delta V_a dt$ and the peak value of the $\int \Delta V_a dt$ is different in every sampling interval due to the change in the dwell times of the voltage vector. Let the maximum value out of these peak values be λ_{max} and it is given as

$$\lambda_{max} = \begin{cases} \frac{\sqrt{3}M}{4f_c}V_{dc}, & 0 \leq M < 1/\sqrt{3} \\ \frac{1}{4f_c}V_{dc}, & 1/\sqrt{3} \leq M < 2/\sqrt{3} \end{cases} \tag{24}$$

For the grid connected applications ($0.9 \leq M \leq 1.1$), the circulating flux component $\phi_{x,c}$ is maximum for the space vector angle ψ_{max} and it is given as

$$\phi_{a,c_{max}} = \phi_{a,c}(t)\,|_{\psi=\psi_{max}} = \frac{V_{dc}}{8Nf_c} \tag{25}$$

and the voltage space vector angle at which this value is achieved is given as

$$\psi_{max} = 120° - \arcsin(\frac{1}{\sqrt{3}M}) \tag{26}$$

The flux in the phase leg is the addition of the $\phi_{a,r}(t)$ and $\phi_{a,c}(t)$ and the $\phi_{a_1}(t)$ could attain its maximum value at $\psi = 0°$, $\psi = 30°$, or $\psi = \psi_{max}$. The values of the flux density in the phase leg at those voltage space vector angles are given in Table I. The maximum value out of these values is used for choosing the cross section area of the phase leg.

Table I: Values of the flux density in the phase leg for different voltage space vector angles

Value	Condition
$B_{a_1}(t)\mid_{\psi=0°} = \frac{(\sqrt{2}+\frac{\beta}{2})V_{dc}}{24Nf_c\beta A_{c,pl}}$	$\psi = 0°$
$B_{a_1}(t)\mid_{\psi=30°} = \frac{\sqrt{3}(\sqrt{2}+\frac{\beta}{2})V_{dc}}{48Nf_c\beta A_{c,pl}} + \frac{V_{dc}}{4Nf_cA_{c,pl}}\left(1-\frac{\sqrt{3}}{2}M_{min}\right)$	$\psi = 30°$
$B_{a_1}(t)\mid_{\psi=\psi_{max}} = \frac{(\sqrt{2}+\frac{\beta}{2})V_{dc}}{24Nf_c\beta A_{c,pl}}\cos\psi_{max} + \frac{V_{dc}}{8NA_{c,pl}f_c}$	$\psi = \psi_{max}$

Simulation and Experimental Results

Time domain simulations and experimental studies have been carried out for the two parallel interleaved VSCs with an interleaving angle of 180°. The total power rating of the system is 3.3 kVA. The switching frequency is taken to be 4.95 kHz. The converter system is connected to the 400V grid and the dc-link voltage is set to 650 V. The fundamental component of the line current is shared equally between the two VSCs. The integrated inductor is designed using the area-product approach to offer the line filter inductance $L_f = 3.8$ mH ($\beta = 0.3$) and the parameters of the inductor are given in Table II. The phase legs and the common leg are made up from ferrite, whereas laminated steel is used for the bridge legs.
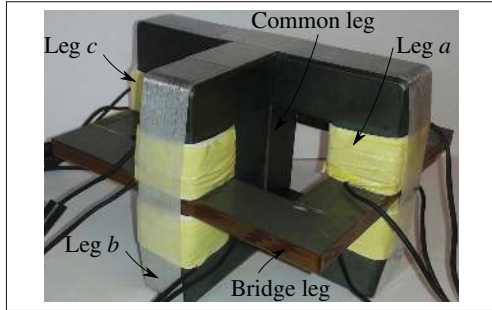
Figure 4: Integrated inductor prototype.

Parameters	Values
Area of the phase leg $A_{c,pl}$	6.45×10^{-4} m^2
Area of the common leg $A_{c,cl}$	6.45×10^{-4} m^2
Area of the bridge leg $A_{c,bl}$	2×10^{-4} m^2
Length of the air gap l_g	5×10^{-4} m
Number of turns N	97

Table II: Design parameters of the Integrated Inductor.

Simulation Results

Simulation results for both the steady-state and the transient conditions are discussed in this sub section.

Steady-state Considerations

Simulated flux density waveforms in the various parts of the magnetic structure of the integrated inductor are shown in Fig. 5. Fig. 5a shows the flux density waveform in the upper limb of one of the phase leg.
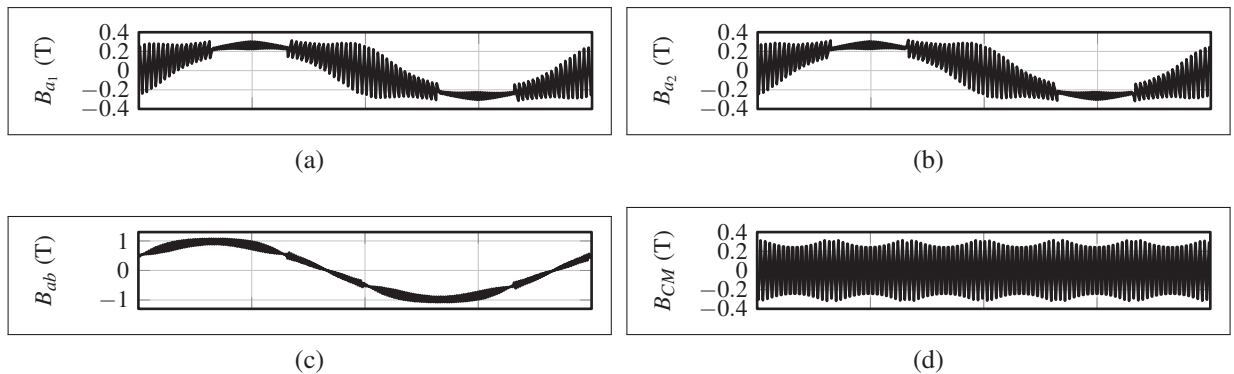
Figure 5: Simulated flux density waveforms. (a) Flux density in the upper limb, (b) Flux density in the lower limb, (c) Flux density in the bridge leg, (d) Flux density in the common leg.

The flux linking with the coils has the resultant flux component and the circulating flux component. The resultant flux component has a dominant harmonic component at the fundamental frequency. It also contains the even multiple of the carrier harmonic components and their side bands. On the other hand,

odd multiple of the carrier harmonic frequency components and their side band harmonic components synthesize the circulating flux. The resultant flux component completes its path through the bridge legs, as shown in Fig. 5c. Fig. 5d shows the flux in the common leg, which has dominant harmonic component at the carrier harmonic frequency.
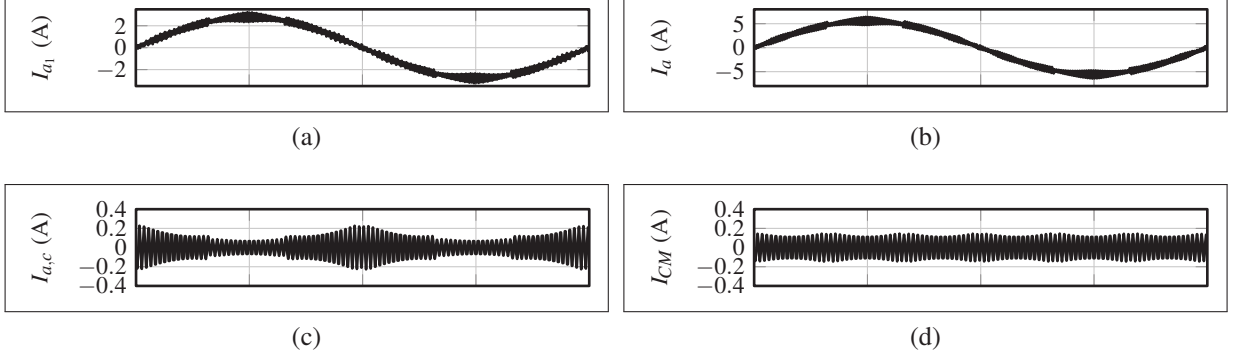

Figure 6: Simulated current waveforms of phase a. (a) Phase a current of VSC$_1$ I_{a_1}, (b) Resultant line current I_a, (c) Phase a circulating current $I_{a,c}$, (d) Common mode circulating current $I_{CM,c}$.

The simulated current waveforms are shown in Fig. 6. The circulating current between the parallel interleaved legs of the phase A is shown in Fig. 6c and it is evident that it is effectively suppressed by the proposed integrated inductor. The resultant line current of phase A is also shown in Fig. 6b and the ripple content in the line current is limited to the desired value. In the steady state, the resultant line current is shared equally between the parallel VSCs and current waveform of one of the VSC$_1$ as shown in Fig. 6a.

Transient Considerations

There is no controlled air gap in the phase legs and the common leg. Therefore, the control scheme should be designed to prevent saturation of the integrated inductor. Asymmetrical regular sampling is used. The feedback signals are sampled and the reference signals are updated at the peak and the valley of the carrier signals, as shown in Fig. 7. For the interleaving angle of 180°, both the VSCs are sampled at the same instant. The strong magnetic coupling between the parallel legs helps in maintaining the equal current sharing in steady-state and sampling the feedback samples at the same instant would ensure voltage second balance. As a result, saturation free operation can be achieved during the transient operation.
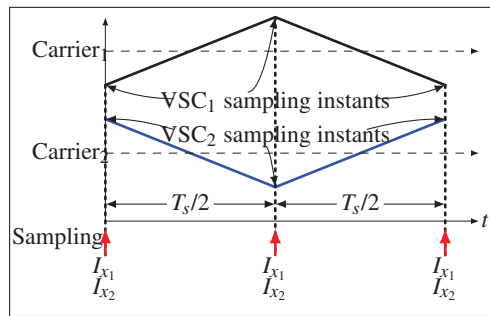

Figure 7: Carrier signals and the sampling instances of both the VSCs with the interleaving angle of 180°.

Individual VSC currents are controlled using the Proportional-Integral (PI) controller. The control variables are transformed in a synchronously rotating frame, which rotates at the fundamental frequency of the grid voltage. The transfer function of the PI controller is given by

$$G_{\mathrm{PI}}(s) = K_p + \frac{K_i}{s} \tag{27}$$

where K_i is the integral gain and the K_p is the proportional gain of the PI controller. The parameters of the PI controller are $K_p = 0.32$ and $K_i = 134.6$. The reference for the active component of the resultant
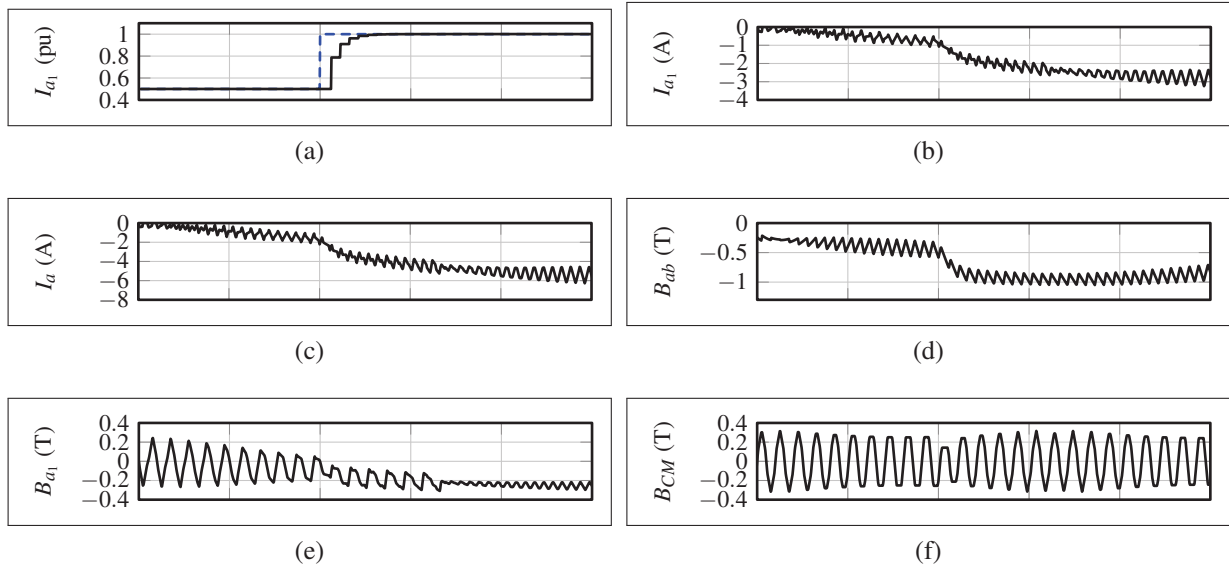
Figure 8: Simulation results during the transient condition, when the reference for the active component of the resultant line current has been changed from 50% of the rated value to 100% of the rated value. (a) Controller performance, (b) Phase a leg current of VSC$_1$ (I_{a_1}), (c) Resultant line current I_a, (d) Flud density in the bridge leg B_{ab}, (e) Flux density in the upper limb of the phase leg B_{a_1}, (f) Flux density in the common leg B_{CM}.

line current has been changed from 50% of the rated value to the 100% of the rated value. The transient response of the d-axis current controller of the VSC$_1$ is shown in Fig. 8a. The individual VSC leg current and the resultant line current are shown in Fig. 8b and Fig. 8c, respectively. The flux density in the phase leg and the common leg are also shown in Fig. 8. As a result of the simultaneous sampling for both the VSCs, a dc component is avoided in the B_{CM} and the integrated inductor operation in the linear part of the B-H curve is ensured. However, inaccuracy in the current measurement sensor (typically $< 1\%$ of the rated current) could lead to an erroneous feedback signal and may introduce dc component in the circulating flux component and the CM flux component. However, the influence of the inaccuracy in the measurement sensor is small and can be neglected for the design purpose.
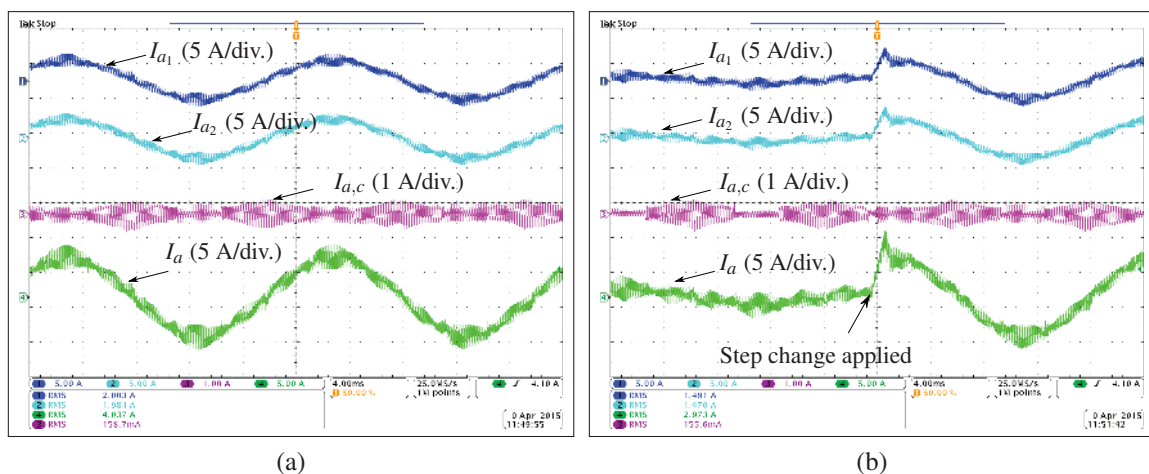
Experimental Results

Figure 9: Experimental results. (a) Steady-state: VSCs are controlled to inject the rated current, (b) Transient considerations: The reference for the injected current is changed from 25% of the rated current to 100% of the rated current.

An integrated inductor prototype was built, as shown in Fig. and the parameters given in Table II. Both the VSCs were connected to the same dc-link and the AC side of these VSCs were connected to the AC

power source MX-35 from California Instruments. The control was implemented using TMS320F28346 floating-point digital signal processor. The experimental waveforms are shown in Fig. 9. Fig. 9a shows the individual currents of each of the inverter, the circulating current between the parallel interleaved VSC legs of that phase and the resultant line current in a steady-state operating conditions. The VSCs were controlled to supply the rated current. As it is evident from Fig. 9a, the ripple in the resultant line current is limited to the desired value and the circulating current between the parallel VSCs is also suppressed effectively by the integrated inductor. The relevant current waveforms during the transient conditions, when the reference current is changed from 25% of the rated value to the 100% of the rated value is shown in Fig. 9b. The circulating current is proportional to the circulating flux component in the integrated inductor. As shown in Fig. 9b, the change in the individual converter current does not influence the circulating current (and therefore the circulating flux component and the CM flux component are also remains unaffected) due to the simultaneous sampling of both the VSCs. As a result of this, the integrated inductor without any controlled air gap in the phase leg and the common leg can be used.

Conclusion

An integrated inductor for two parallel interleaved VSCs is proposed. A four leg magnetic structure is used. The integrated inductor combines the functionalities of both the line filter inductor and the circulating current inductor. Both the parallel VSCs are modulated using the 60° discontinuous modulation scheme. For the unity power factor applications, the resultant flux component achieves its maximum value when the value of the circulating flux component is very small and vice-versa. As a result, substantial size reduction can be achieved. A sampling scheme for both the VSCs along with the controller design has been also discussed. The steady-state and the transient performance of the system are also verified by the simulations and the experimental results.

References

[1] R. Jones and P. Waite, "Optimised power converter for multi-MW direct drive permanent magnet wind turbines," in *Proc. European Conference on Power Electronics and Applications (EPE 2011)*, Aug 2011, pp. 1–10.

[2] G. Gohil, L.Bede, R.Teodorescu, T. Kerekes, and F. Blaabjerg, "Line filter design of parallel interleaved VSCs for high power wind energy conversion system," *IEEE Trans. Power Electron.*, [Online early access], DOI: 10.1109/TPEL.2015.2394460, 2015.

[3] F. Ueda, K. Matsui, M. Asao, and K. Tsuboi, "Parallel-connections of pulsewidth modulated inverters using current sharing reactors," *IEEE Trans. Power Electron.*, vol. 10, no. 6, pp. 673–679, Nov 1995.

[4] D. Zhang, F. Wang, R. Burgos, L. Rixin, and D. Boroyevich, "Impact of Interleaving on AC Passive Components of Paralleled Three-Phase Voltage-Source Converters," *IEEE Trans. Power Electron.*, vol. 46, no. 3, pp. 1042–1054, 2010.

[5] J. Prasad and G. Narayanan, "Minimization of Grid Current Distortion in Parallel-Connected Converters Through Carrier Interleaving," *IEEE Trans. Ind. Electron.*, vol. 1, no. c, pp. 1–1, 2013.

[6] I. G. Park and S. I. Kim, "Modeling and analysis of multi-interphase transformers for connecting power converters in parallel," in *Proc. of 28th Annual IEEE Power Electronics Specialists Conference, 1997. PESC '97*, vol. 2, Jun 1997, pp. 1164–1170 vol.2.

[7] R. Hausmann and I. Barbi, "Three-phase multilevel bidirectional dc-ac converter using three-phase coupled inductors," in *Proc. IEEE Energy Conversion Congress and Exposition, 2009. ECCE 2009.*, Sept 2009, pp. 2160–2167.

[8] F. Forest, E. Laboure, T. Meynard, and V. Smet, "Design and comparison of inductors and intercell transformers for filtering of PWM inverter output," *IEEE Trans. Power Electron.*, vol. 24, no. 3, pp. 812–821, 2009.

[9] J. Salmon, J. Ewanchuk, and A. Knight, "PWM inverters using split-wound coupled inductors," *IEEE Trans. Ind. Appl.*, vol. 45, no. 6, pp. 2001–2009, 2009.

[10] G. Gohil, R. Maheshwari, L. Bede, T. Kerekes, R. Teodorescu, M. Liserre, and F. Blaabjerg, "Modified discontinuous pwm for size reduction of the circulating current filter in parallel interleaved converters," *IEEE Trans. Power Electron.*, vol. 30, no. 7, pp. 3457–3470, July 2015.

[11] G. Gohil, L. Bede, R. Maheshwari, R. Teodorescu, T. Kerekes, and F. Blaabjerg, "Parallel interleaved VSCs: influence of the PWM scheme on the design of the coupled inductor," in *Proc. 40th Annual Conference on IEEE Industrial Electronics Society, IECON 2014*, Oct 2014, pp. 1693–1699.